Evolution of Charge Trapping and Insulating Performances of Epoxy Materials Containing Hydrolyzable Chlorine During Hygrothermal Aging

Yushun Zhao, Yufan Xu, Cheng Yan, Gilbert Teyssedre, Bin Du

Evolution of Charge Trapping and Insulating Performances of Epoxy Materials Containing Hydrolyzable Chlorine during Hygrothermal Aging

Yushun Zhao*, Yufan Xu*, Cheng Yan*, Gilbert Teyssèdre, and Bin Du***
*Electrical Engineering Department, Hefei University of Technology, Hefei, Anhui, 230009 China
**LAPLACE, University of Toulouse, 118 route de Narbonne, F-31062 Toulouse Cedex 9, France

To cite: Y. Zhao, Y. Xu, H. Shen, B. Du, G. Teyssèdre, "*Evolution of Charge Trapping and Insulating Performances of Epoxy Materials Containing Hydrolyzable Chlorine during Hygrothermal Aging*", IEEE Trans. Dielectr. Electr. Insul. 29, 1828-1837, 2022
DOI: 10.1109/TDEI.2022.3197111

***Abstract*—Hydrolyzable chlorine is a well-known residue issued from the synthesis of epoxy resin, which may impart specific dielectric properties. In this work, the changes in distributed energy levels and charge trap depths of the molecule containing such defects are investigated using quantum chemical calculations. These changes are analyzed from the microscopic perspectives of electron energy structure and electron cloud offset. The charge transport and charge injection behavior in epoxy materials before and after the hydrolysis are predicted using the analysis results. The volume resistivities and space charges of epoxy materials with three different hydrolyzable chlorine contents are tested at different hygrothermal aging times, which are consistent with the previous predictions. These results are used to explain the AC breakdown strength of these epoxy materials at different hygrothermal aging times. It is indicated that the structural changes (electronegativity and atomic position changes) of the molecule containing hydrolyzable chlorine before and after hydrolysis change the spatial distribution of electron cloud density between and on valence bonds, and in turn change the energy levels of different molecular segments. This results in a large increase in the overall electron trap depth and a small decrease in the overall hole trap depth of the molecule after hydrolysis.**

***Index Terms*—Chlorine, energy level distribution, epoxy resin, quantum calculation, space charge, trap depth**

I. Introduction

Epoxy resin has been widely used in the electronic device packaging and the main insulation of high voltage equipment considering its excellent electrical performances [1-4]. Epoxy resins are generally prepared by the reaction of epichlorohydrin with active hydrogen-containing compounds forming chlorine [5]. The formed chlorine acts as a chain terminal and is hydrolyzable, thus causing drawbacks such as a decrement of mechanical strength due to loss of crosslink density and corrosion of metals in the equipment. The hydrolyzable chlorine should have been removed. However, a small amount of hydrolyzable chlorine remains in the final production. The chlorine has a negative impact on the electrical insulation property of the epoxy system. It has been reported that the AC treeing propagation rate of the high-chlorine epoxy system is higher than that of the low-chlorine epoxy system, and the AC breakdown time of the high-chlorine epoxy system is lower than that of the low-chlorine epoxy system [5].

Hydrolyzable chlorine exists as a chemical impurity in epoxy resins. The chlorine atom impurity is easily hydrolyzed into hydroxyl group. Before and after hydrolysis, the difference in electron affinity of the elements causes a change of electron density in the molecules containing hydrolyzable chlorine. That may change the charge trap depths and electron energy structure of the molecules, thus resulting in the different charge transport and charge injection behaviors in epoxy materials.

Many scholars have investigated the effects of chemical impurities in polymer dielectrics on the charge transport and charge injection by combining quantum chemical calculation and experiments [6-8]. T. Takada et al investigated the effect of small oxide polyethylene (PE) molecular chain in low density polyethylene (LDPE) on charge transport using a space charge measurement system and quantum chemical calculation. The results show that the ketone group in the oxide PE molecular chain produces a hole trap site (trap depth is 0.85 eV). That causes the holes in LDPE to drift slowly toward the cathode and accumulate at the equilibrium position in the electric field [9]. M. El-Shahat et al compared the effect of chemical impurities (including carbonyl, vinyl, and conjugated double bond impurities) on charge injection barriers at copper/PE interface using computational quantum mechanics. It was found that the terminal carbonyl and conjugated double bond produce the lowest injection barrier for electrons and holes, respectively [10]. J. Li et al investigated the effect of remnant unreacted amine-type hardener on charge injection at the electrode/resin interface using pulsed electro-acoustic method and quantum chemical calculation. The results show that the remnant hardener impurities lead to a low hole injection barrier. That makes holes easily be injected into amine from anode electrode

and subsequently transport to accumulate in the vicinity of cathode electrode [11].

In this paper, using quantum chemical calculation, we first analyzed the changes in distributed energy levels and charge trap depths of the molecule containing hydrolyzable chlorine before and after hydrolysis. These were analyzed from the microscopic perspectives of electron energy structure and electron cloud offset. Then the analysis results were used to predict the charge transport as well as charge injection behavior of epoxy materials. To validate the results of above theoretical analysis, the volume resistivities and space charges of epoxy samples were tested at different hygrothermal aging times. In addition, we also tried to use the theoretical analysis to explain the AC breakdown strength results of these epoxy samples at different hygrothermal aging times, expecting to provide a theoretical reference for the modulation of chemical impurities on the electrical properties of materials.

II. Theoretical Analysis

A. Hydrolysis Process of Acid Anhydride/Chlorohydrin Ether Molecule

We take the molecule containing hydrolyzable chlorine (chlorohydrin ether molecule) in bisphenol-A type epoxy resin (DGEBA) as an example. Here we compare the structure of chlorohydrin ether molecule with that of DGEBA molecule. By opening the ring of an epoxy group in DGEBA molecule and connecting a chlorine atom to the methylene group after ring-opening, the chlorohydrin ether molecule can be obtained. During the cross-linking reaction between DGEBA and acid anhydride hardener, the chlorohydrin ether molecule will also cross-link with the acid anhydride molecule due to the presence of epoxy group at one end. The acid anhydride hardener here is methyltetrahydrophthalic anhydride (Me-THPA). Fig. 1b-1 shows the structure of acid anhydride/chlorohydrin ether molecule formed by cross-linking, which is called "AH-Cl". R_1 is the Me-THPA after opening the five-membered ring.

The thermal hydrolysis of haloalkanes will release HX (X = Cl, Br, I) [12]. Thus, the AH-Cl molecule, as a chlorinated alkane, releases hydrogen chloride (HCl) upon its thermal hydrolysis. Fig. 1a shows the hydrolysis process of the AH-Cl molecule. Fig. 1b-2 is the hydrolyzed structure of the AH-Cl molecule, which is called "AH-OH". It can be seen that the difference between the structures of AH-Cl molecule and AH-OH molecule is only reflected in the structure of molecular segment C. Specifically, compared with AH-Cl molecule, the chlorine atom in the segment C is replaced by the hydroxyl group in AH-OH molecule.

The electronegativity of an element comprehensively considers the electron affinity and ionization energy, and its magnitude is determined by factors such as the number of atomic nuclear charges and electron layers of the element. The electronegativity of oxygen atom (3.44, relative value) is slightly greater than that of chlorine atom (3.16, relative value), so the electron density on the valence bonds will slightly reduce after the chlorine atom in segment C is replaced by the hydroxyl group. That may increase the HOMO energy level of segment C. The shielding effect of shared electron pair in hydroxyl group greatly weakens the attraction of the oxygen nucleus to the outer electrons, so the electron density between the valence bonds will decrease after the chlorine atom in segment C is replaced by the hydroxyl group. That may make the LUMO energy level of segment C higher. The quantification of energy level changes is obtained using quantum chemical calculation, as shown in the following section.

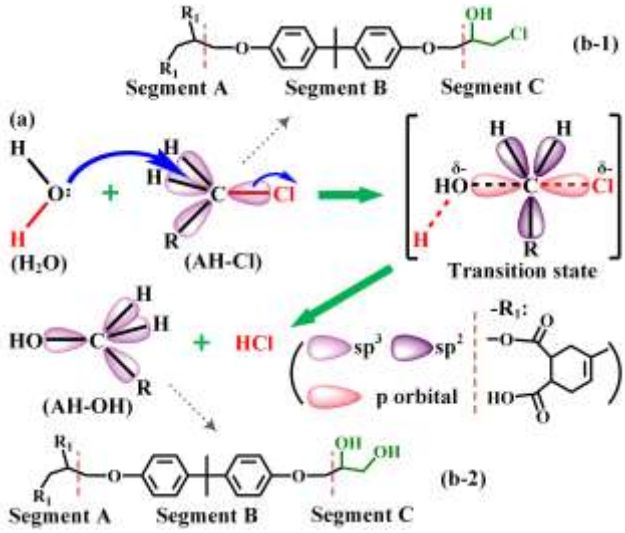

Fig. 1. Hydrolysis diagram of acid anhydride/chlorohydrin ether molecule.

B. Distributed Energy Levels and Charge Trap Depths of AH-Cl and AH-OH Molecules

The AH-Cl and AH-OH molecules constructed here are both low molecular weight polymers composed of two Me-THPA monomers and one chlorohydrin ether monomer, and their structures are also shown in Fig. 2a and Fig. 3a, where the structure of R_1 is the same as in Fig. 1. We used DFT with Gaussian 09 software to optimize the geometrical structures of AH-Cl and AH-OH oligomer molecules, respectively. The B3LYP hybrid functional method and 6-31G (d) basis function set, which are widely adopted for the simulation of low molecular weight polymers [13], were used in the calculations. The program keyword was set to "# opt b3lyp/6-31 g(d) geom=connectivity". The "charge" and "multiplicity" were set to "0" and "1", respectively. After the optimization, the output file of type "chk" was obtained. After opening the output file with GaussView software, we checked the bond angles through the "Angle properties" function and the energy level information through the "MOs" function. Fig. 2 and Fig. 3 show the energy band structure and distributed energy levels of the AH-Cl and AH-OH oligomer molecules, respectively. The zero levels in both figures are the vacuum levels (VL).

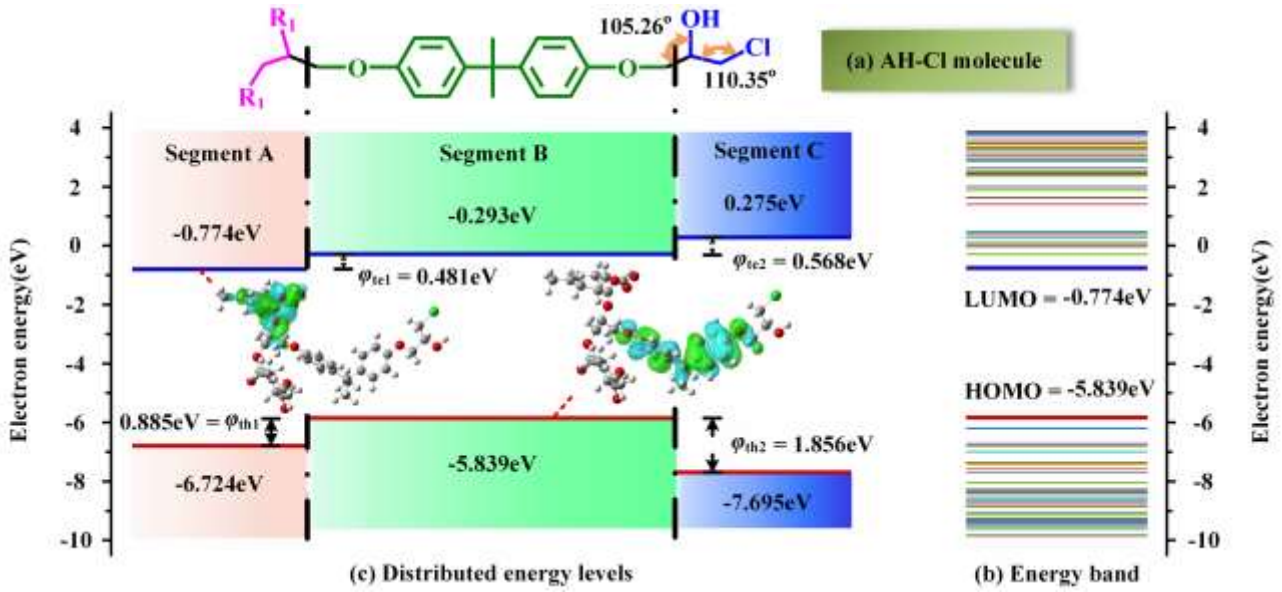

Fig. 2. The energy band structure and distributed energy levels of AH-Cl molecule.

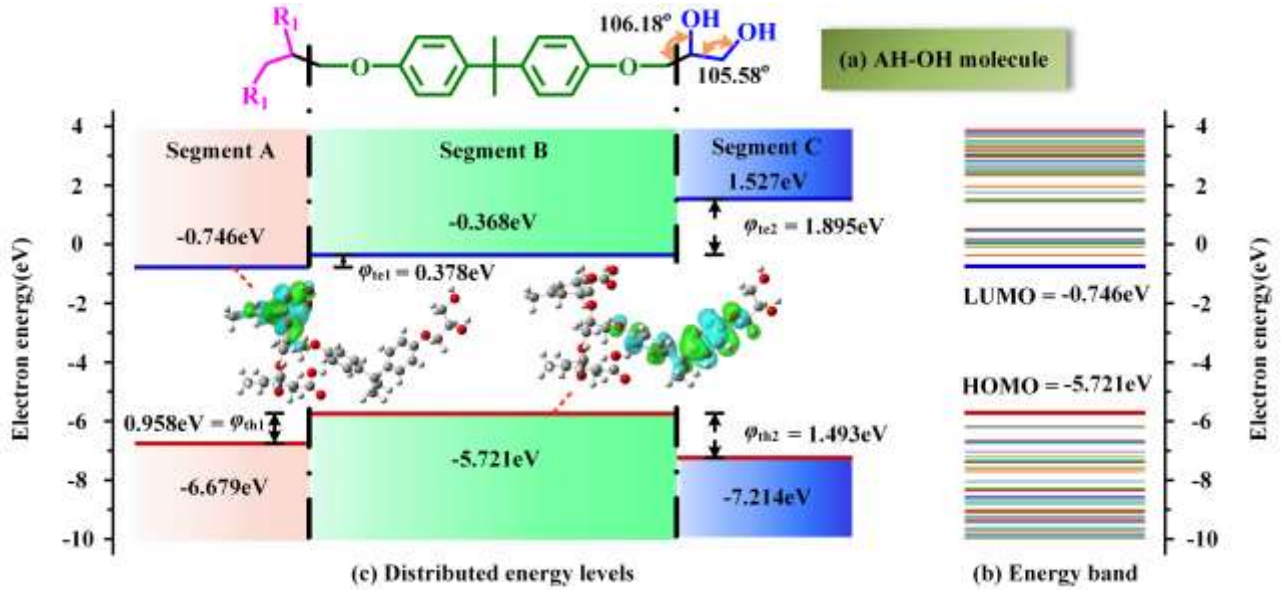

Fig. 3. The energy band structure and distributed energy levels of AH-OH molecule.

Fig. 2b shows the energy band structure of the AH-Cl molecule. The molecule orbital is locally distributed along the molecular chain if we focus on an energy level. Thus, we can obtain the distributed energy levels of AH-Cl molecule on different segments, as shown in Fig. 2c. It can be seen that the LUMO energy level of segment A is that of the whole AH-Cl molecule, and the HOMO energy level of segment B is that of the whole AH-Cl molecule. The distributions of molecular orbitals corresponding to the LUMO and HOMO energy levels are shown in Fig. 2c. If an excess electron trapped at the LUMO level of a segment drifts towards its adjacent segment under an electric field, the trapped electron must overcome an energy barrier. This means that the LUMO level of the segment is a trapping site for an electron, and the barrier height is the electron trap depth generated by the site [10]. Likewise, if an excess hole trapped at the HOMO level of a segment drifts towards its adjacent segment under an electric field, the trapped hole must overcome an energy barrier. This means that the HOMO level of the segment is a trapping site for a hole, and the barrier height is the hole trap depth generated by that site. As shown in Fig. 2c, the LUMO energy levels of segment A and segment B are both electron trapping sites of the AH-Cl molecule. The electron trap depths they generate are φ_{te1} (0.481 eV) and φ_{te2} (0.568 eV), respectively. The HOMO energy level of segment B is a hole trapping site. When the excess holes trapped by the site drift towards segment A and segment C under an electric field, they need to overcome an energy barrier, which is φ_{th1} (0.885eV) and φ_{th2} (1.856eV), respectively.

Fig. 3b and Fig. 3c show the energy band structure and distributed energy levels of AH-OH molecule, respectively. The distribution of molecular orbitals corresponding to the LUMO and HOMO energy levels, the electron trap depths, and the hole trap depths are also shown in Fig. 3c. Compared with the electron trap depths of AH-Cl molecule, a small decrease

(by 0.103 eV) in φ_{te1} and a large increase (by 1.327 eV) in φ_{te2} occurred for the AH-OH molecule. Compared with the hole trap depths of AH-Cl molecule, a slight increase (by 0.073 eV) in φ_{th1} and a small decrease (by 0.363 eV) in φ_{th2} occurred for the AH-OH molecule. The changes in charge trap depths are affected precisely by the distributed energy levels, so we next compare the distributed energy levels of the two molecules.

It can be seen that after the hydrolysis of AH-Cl molecule, the segment C shows a large increase (by 1.252 eV) in LUMO energy level and a small increase (by 0.481 eV) in HOMO energy level; the segment B shows a slight decrease (by 0.075 eV) in LUMO energy level and a slight increase (by 0.118 eV) in HOMO energy level; the segment A almost shows no changes in LUMO and HOMO energy levels.

C. Analysis of Changes in Distributed Energy Levels

When the oxygen atom in the hydroxyl group is bonded to the hydrogen atom in the hydroxyl group, the shared electron pair is strongly biased towards the oxygen atom side due to the large difference between the electronegativity of the oxygen atom (3.44, relative value) and that of the hydrogen atom (2.1, relative value). The shielding effect of this shared electron pair greatly weakens the attraction of the oxygen nucleus to the outer electrons. Consequently, even if the electronegativity of the oxygen atom is slightly larger than that of the chlorine atom (3.16, relative value), the attraction of the electronegative element in segment C to the orbital electrons between the valence bonds is reduced after the chlorine atom in segment C is replaced by the hydroxyl group. This causes the electron cloud density between the nucleus of electronegative element and the nucleus of the atom whose orbital electrons have shifted decrease. The system of electron orbitals between the valence bonds becomes more unstable, and the energy of the system is elevated. Thus, the LUMO energy level of segment C will increase after the AH-Cl molecule is changed to the AH-OH molecule. In addition, The C-C-Cl bond angle in segment C of the AH-Cl molecule is 110.35° (shown in Fig. 2a), and the C-C-O bond angle in segment C of the AH-OH molecule is 105.58° (shown in Fig. 3a). Compared to the chlorine atom in segment C of the AH-Cl molecule, the oxygen atom of the hydroxyl group in segment C of the AH-OH molecule is closer to the other atoms in segment C. The electron orbitals of the oxygen atom are more easily hybridized with those of the other atoms in segment C. As a result, the average radius of the electron orbitals involved in the hybridization between the valence bonds in segment C increases, the potential energy of the orbital electrons rises. Therefore, after the AH-Cl molecule is transformed into the AH-OH molecule, the LUMO energy level of the segment C shows a large increase.

Due to the electronegativity difference between elements, the orbital electrons on the O-C polar covalent bond are shifted towards the position of oxygen atom, and the orbital electrons on the Cl-C polar covalent bond are shifted towards the position of chlorine atom. Since the electronegativity of oxygen element is larger than that of the chlorine element, the polarity of the O-C covalent bond is stronger than that of the Cl-C covalent bond, which makes the offset degree of the orbital electrons on the O-C covalent bond larger than that of the orbital electrons on the Cl-C covalent bond. In the segment C of AH-Cl molecule, there is an O-C polar covalent bond and a Cl-C polar covalent bond. While in the segment C of AH-OH molecule, there are two O-C polar covalent bonds. Thus, the offset degree of the orbital electrons on valence bonds in segment C becomes larger after the AH-Cl molecule is transformed into AH-OH molecule. This causes the electron cloud density on valence bonds decrease, so the overlap of the electron cloud decreases. The covalent bonds formed between bonding atoms become more unstable and the energy of the electron orbital system on valence bonds is elevated. Therefore, the HOMO energy level of segment C shows a small increase.

In the AH-Cl molecule, the 2p orbitals of the oxygen atoms in ether oxygen groups connected to the benzene rings and the 2p orbital of the oxygen atom in the hydroxyl group form p-π conjugation with the large π orbitals of the benzene rings. This makes the electron cloud density between the conjugated atoms in the conjugated system decrease and the internal energy of the system lower, so the conjugated system formed is relatively stable. In optimized AH-Cl molecule, the C-C-O bond angle formed by the two carbon atoms connecting segment B and segment C and the oxygen atom in hydroxyl group of segment C is 105.26°, as shown in Fig. 2a. The C-C-O bond angle increases to 106.18° after the AH-Cl molecule is transformed into AH-OH molecule, which indicates a slight shift of the oxygen atom in the hydroxyl group of segment C away from the segment B. As a result of the shift, the conjugation between the 2p orbital of the oxygen atom in the hydroxyl group of segment C and the large π orbitals of the benzene rings in segment B is weakened. This leads to a slight increase in the electron cloud density of the original conjugated system in segment B, and the original conjugated system becomes more unstable. In this way, the energy of the conjugated system in segment B increases slightly, and the HOMO energy level of segment B also has a slight increase. Since the bond length of the C-O covalent bond (1.43 Å) is shorter than that of the C-Cl covalent bond (1.82 Å), after the chlorine atom is replaced by a hydroxyl group, the distance between the oxygen atom of the hydroxyl group and the segment B is reduced, and the repulsion between the extranuclear electrons of the oxygen atom and the antibonding π orbital electrons in segment B becomes stronger. This makes the average motion radius of the orbital electrons moving around the orbital center in the antibonding orbital slightly smaller, and the energy of the electrons in antibonding orbital is slightly reduced. Therefore, there is a slight decrease in the LUMO energy level of the segment B.

The attraction for electrons by electronegative elements is a kind of electrostatic interaction that rapidly weakens and eventually disappears with the increase of the carbon chain length. Consequently, the substitution of the electronegative element in segment C has little effect on the LUMO and HOMO energy levels of segment A.

D. Effect of Charge Trap Depth Variations on Charge Transport

Numerous works have pointed out that deep levels favor the

trapping of electrons or holes, leading to the accumulation of space charges. On the contrary, shallow traps favor the de-trapping of electrons or holes, leading to a slight charge accumulation. In this section, we analyze the effect of changes in charge trap depths on the charge transport.

In order to observe a clear change in charge distribution, two excess electrons were introduced into the AH-Cl molecule and the AH-OH molecule, respectively. Recalculating the charge distribution using DFT with Gaussian 09 software, we obtained the Mulliken atomic charges (the effective electric charge distribution of protons and orbital electrons) in these molecules. The total Mulliken atomic charges on different segments of AH-Cl and AH-OH molecules are shown in Fig. 4.

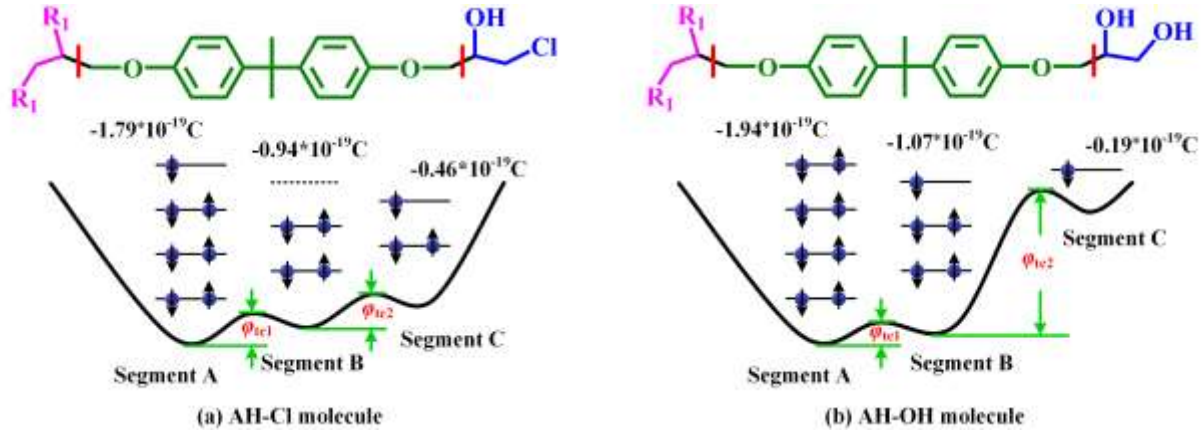

Fig. 4. The distribution of Mulliken atomic charges in AH-Cl and AH-OH molecules.

As described previously, the LUMO energy levels of both segment A and segment B are electron trapping sites. However, since the LUMO energy level of segment A is lower than that of segment B, the LUMO energy level of segment A will trap electrons more easily than that of segment B. As shown in Fig. 4a and Fig. 4b, the total Mulliken atomic charges on segment A are always more than that on segment B for both AH-Cl and AH-OH molecules. The φ_{te1} of the AH-OH molecule is smaller than that of the AH-Cl molecule, so the electrons in the AH-OH molecule are more easily transferred from segment A to segment B. It can be seen from Fig. 4 that the total Mulliken atomic charges on segment B of the AH-OH molecule increase compared with that on segment B of the AH-Cl molecule. While the φ_{te2} of the AH-OH molecule is larger than that of the AH-Cl molecule, the electrons in segment B of the AH-OH molecule are difficult to be transferred to segment C, so the total Mulliken atomic charges on segment C of the AH-OH molecule is less than that on segment C of the AH-Cl molecule.

Also, the charge trap depths in the molecule affect the hopping probability of the charges trapped at the trapping sites, thus affecting the carrier mobility in the transport process and the electrical resistivity of the material. Their relationships are shown in (1), (2) and (3), where θ_{hop} is hopping probability, φ_t is charge trap depth, k is the Boltzmann constant, T is absolute temperature, μ is carrier mobility, μ_0 is intrinsic mobility, ρ is electrical resistivity, n is electron concentration, q is electron charge quantity, μ_n is electron mobility, p is hole concentration, μ_p is hole mobility.

$$\theta_{hop} = \exp(-\varphi_t / kT) \quad (1)$$

$$\mu = \mu_0 \theta_{hop} \quad (2)$$

$$\rho = (nq\mu_n + pq\mu_p)^{-1} \quad (3)$$

Compared with that of the AH-Cl molecule, the overall electron trap depth φ_{te} shows a large increase (by 1.224 eV, which is the difference between 1.327 eV and 0.103 eV) and the hole trap depth φ_{th} shows a small decrease (decrease by 0.29 eV, which is the difference between 0.363 eV and 0.073 eV) for the AH-OH molecule. Since the increasing magnitude of the electron trap depth is much larger than the decreasing magnitude of the hole trap depth, the change in the electron trap depth becomes the main factor determining the change in the resistivity of the material. It can be seen from (1) and (2) that a large increase in φ_t will lead to a decrease in the electron hopping probability, resulting in a low electron mobility μ_n. According to (3), the resistivity ρ of the material will increase after the AH-Cl molecule is transformed into AH-OH molecule.

E. Charge Injection at the Electrode/Material Interfaces

In this section, the charge injection parameters are calculated to discuss charge transfer at the electrode/material interfaces. The electrodes here are aluminum (Al) and semiconductor (SC). Based on the electrode/material interface properties [14-15], the electron injection barrier Φ_{Be} and the hole injection barrier Φ_{Bh} at the Al electrode and the SC electrode can be calculated.

Fig. 5 shows the charge injection and transfer of the electrode/AH-Cl system before and after contact. The VL here is the reference energy level. The Fermi level (E_F) is defined as the middle position of the LUMO-HOMO gap. The Φ_{Al} is the work function of the Al electrode (4.25 eV) and the Φ_{SC} is the work function of the SC electrode (5.56 eV) [16]. As shown in Fig. 5a, the E_F of AH-Cl is higher than that of Al and SC electrodes before the contact. Hence, when the AH-Cl contacts with the electrodes, the electrons of AH-Cl will move into Al and SC electrodes, and the E_F of AH-Cl tends to be the same with that of the electrodes. The migration direction of the electrons is shown in Fig. 5a. After contact, as shown in Fig. 5b, the distance (Zc) becomes small. Here we set Zc=3.7 Å because the adsorption energy is the minimum value [17-19].

Electrons transfer from the AH-Cl into the Al and the SC electrodes, leading to the formation of positive charges on the surface of AH-Cl and of negative charges on the surface of Al and SC electrodes. The VL shifts at both interfaces to keep all E_F levels coincide with each other. Compared with that at the Al/AH-Cl interface, the VL at the SC/AH-Cl interface shifts to a much lower value due to a large E_F difference (ΔE_{F2}) between the SC and the AH-Cl. Consequently, the electron injection barriers are reduced. While the hole injection barriers after contact keep the same value with that before contact due to the created energy sites by surficial positive charges of the AH-Cl. According to (4) and (5), the charge injection barriers at the electrode/AH-Cl interfaces calculated after the contact are listed in Table. I.

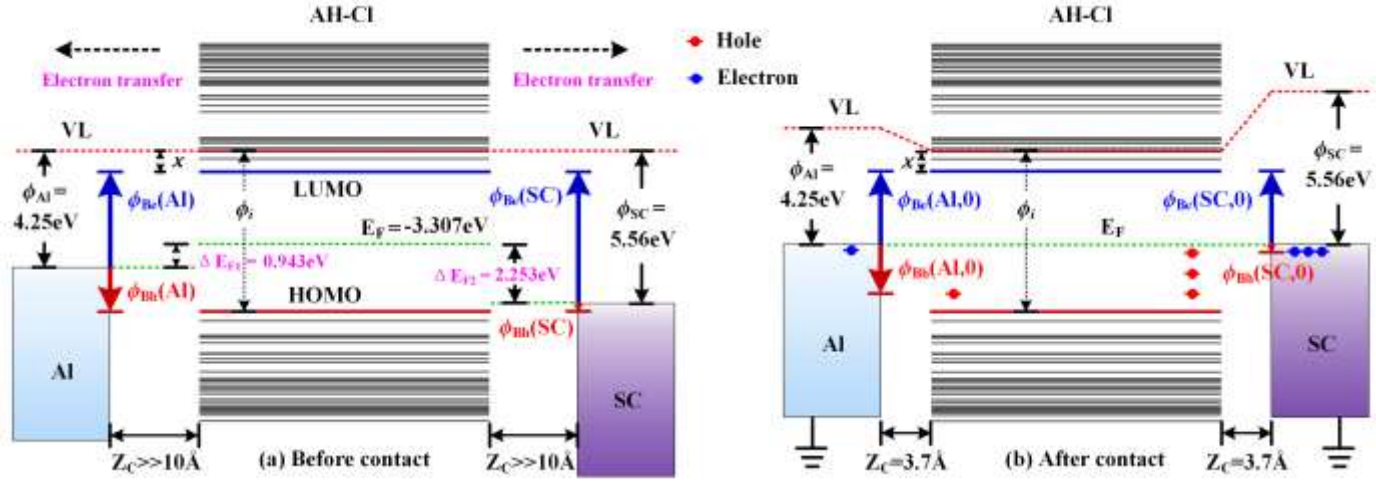

Fig. 5. Charge injection and transfer before and after contact of electrode/AH-Cl system; (a) before contact; (b) after contact.

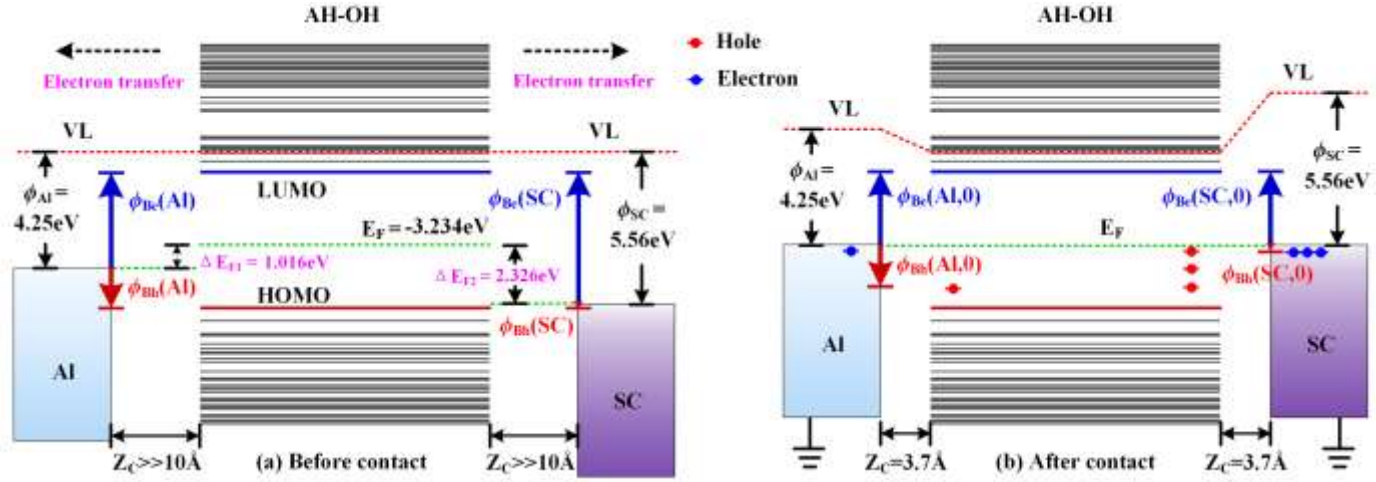

Fig. 6. Charge injection and transfer before and after contact of electrode/AH-OH system; (a) before contact; (b) after contact

$$\phi_{Be} = \phi_{WM} - \chi - \Delta E_F \quad (4)$$

$$\phi_{Bh} = \phi_i - \phi_{WM} \quad (5)$$

where Φ_{WM} is the work function of electrode material, χ is the electron affinity (energy difference between the VL and the LUMO level), Φ_i is the ionization energy (energy difference between the VL and the HOMO level).

Similar to that of the electrode/AH-Cl system, the charge injection and transfer before and after contact of electrode/AH-OH system can be discussed, as shown in Fig. 6. The charge injection barriers at the electrode/AH-OH interfaces calculated after the contact are also listed in Table. I.

Due to the high Φ_{Be} (Al, 0) of both electrode/AH-Cl system and electrode/AH-OH system, it is difficult for electrons to be injected from the Al electrode under a low electric field. However, the Φ_{Bh} (SC, 0) of both electrode/AH-Cl system and electrode/AH-OH system is low. The holes would be easily injected from SC electrode into AH-Cl and AH-OH even under a low electric field and subsequently transport to the opposite electrode. Thus, we can apply a low positive polarity voltage to the SC electrode when measuring the space charges. By comparing the transport behavior of positive charges inside the two materials and combining with the trapping sites in the chemical structure calculated above, the mechanism of the hole trap depths on the hole migration can be investigated. The specific experiments are described below.

TABLE I
CALCULATED CHARGE INJECTION PARAMETERS

Electronic properties	AH-Cl	AH-OH
LUMO	-0.774 eV	-0.746 eV
HOMO	-5.839 eV	-5.721 eV
After contact Φ_{Be} (Al,0)	2.533 eV	2.488 eV
After contact Φ_{Bh} (Al,0)	1.589 eV	1.471 eV
After contact Φ_{Be} (SC,0)	2.533 eV	2.488 eV
After contact Φ_{Bh} (SC,0)	0.279 eV	0.161 eV

III. EXPERIMENTAL VERIFICATION

A. Raw Materials and Sample Preparation

One of the bisphenol-A type epoxy resin is branded as YD-126D. It is chemically pure, with an epoxy value of 0.580 mol/100g and a hydrolyzable chlorine content of 120 ppm. Another bisphenol-A type epoxy resin is branded as 128SD. It is chemically pure, with an epoxy value of 0.463 mol/100g and a hydrolyzable chlorine content of 26145 ppm. Curing agent: Me-THPA, chemically pure. All experimental epoxy resins and the curing agent were purchased from Huntsman Polyurethanes (China) Ltd. Curing accelerator: N, N-dimethylbenzylamine (BDMA), purchased from Shanghai Aladdin Biochemical Technology Co., Ltd. By mixing and formulating the above two different brands of bisphenol-A type epoxy resins, we obtained the epoxy resins with the hydrolyzable chlorine content of about 120 ppm, 500 ppm and 900 ppm, respectively. The actual hydrolyzable chlorine contents in the formulated epoxy resins were tested, which were 120 ppm, 437 ppm, and 783 ppm, respectively. Equation (6) is the formula for calculating the mass of the Me-THPA used in curing reaction per 100g of epoxy resin, in where W_h is the relative molecular weight of Me-THPA, E_v is the epoxy value of each epoxy resin used, k is the correction coefficient (taken as 1 in this experiment).

$$\text{Anhydride dosage} = W_h * E_v * k \tag{6}$$

Table II shows the curing formulations of epoxy/Me-THPA systems with three different hydrolyzable chlorine contents. The mass of BDMA added was 0.6 % (1.38 g) of the mass of epoxy resin in the three curing systems. According to the formulations in Table II, the two brands of epoxy resin and the Me-THPA were weighed and poured into the reaction kettle in turn. We dispersed the mixture evenly with a high-speed disperser at a constant temperature of 353.15 K, and simultaneously performed a continuous vacuum defoaming treatment. After high-speed dispersion for 20 minutes, the accelerator BDMA was added to the reactor and continued high-speed dispersion and vacuum defoaming treatment. After 5 minutes, we poured the resin castable into the mold (before casting, the mold should be preheated in a drying oven at 353.15 K for at least 3 hours). We vacuumed a constant temperature oven for 5 minutes after putting the casted mold into the oven. Lastly, the epoxy castable was cured at a constant temperature of 373.15 K for 3 hours and at a constant temperature of 403.15 K for 12 hours to obtain the cured epoxy samples.

According to JESD22-A102-C test standard, we subjected the epoxy samples to hygrothermal aging treatment for 0 hour, 24 hours, 48 hours, and 96 hours under the conditions of 100 % R.H humidity, 394.15 K temperature, and 205 kPa steam pressure using constant temperature and humidity aging test chamber. After that, the volume resistivity, space charge density, and AC breakdown strength were tested. Prior to testing, the epoxy samples were placed in a vacuum drying oven at 323.15 K for 24 hours in order to remove moisture and any volatile substances.

TABLE II
FORMULATIONS OF EPOXY CURING SYSTEMS

Hydrolyzable chlorine content/ppm	Epoxy resin/g		Me-THPA/g
	YD-126D	128SD	
120	230	0	221.67
437	226.64	3.36	221.02
783	223.11	6.89	220.33

B. Volume Resistivity Test

The epoxy samples used for volume resistivity test are discs with a diameter of 10 cm and a thickness of 1 mm. We selected five groups of epoxy samples from each of the hydrolyzable chlorine content, and tested the volume resistivity of the samples after different hygrothermal aging times. The five groups of samples were of uniform thickness and smooth surfaces. Under the same temperature and air humidity, the resistivity test was conducted on a high resistance meter. The test electrodes are a three-electrode system in the form of circular plates, the applied voltage is DC 1000 V, and the charging time is 15s. Here we added error bars to show the standard deviation of the test data.

C. Space Charge Test

The space charge distributions of epoxy samples with a hydrolyzable chlorine content of 783 ppm were measured at room temperature using a PEA system, respectively, without hygrothermal aging and after 48 hours of hygrothermal aging. An Al electrode was chosen as a ground electrode, and a SC layer was used between the high voltage electrode and the tested samples. When testing these two kinds of samples, the DC voltage of +10 kV was applied to the high voltage electrode. The samples used for space charge test are discs with a diameter of 5 cm and a thickness of 700 μm.

D. AC Breakdown Voltage Test

The epoxy samples used for AC breakdown voltage test are discs with a diameter of 10 cm and a thickness of 1 mm. The breakdown voltages of the epoxy samples were tested according to GB/T1408.1-2016 test standard. The test power supply was a high voltage testing transformer with a frequency of 50 Hz, and the test electrodes were two identical spherical electrodes with a diameter of 20mm. Five groups of samples with uniform thickness and smooth surfaces were selected from each hydrolyzable chlorine content and hygrothermal aging time to test the AC breakdown voltage. During the test, the samples and test electrodes were immersed in insulating oil, and the output voltage of testing transformer was uniformly increased with the ramping up rate of 2000 V/s.

In addition, the test data were fitted by a two-parameter Weibull distribution model. Equation (7) is the expression of

the probability distribution function for the two-parameter Weibull distribution model, where α is the scale parameter, reflecting the breakdown strengths of the samples when the breakdown probability is 63.2%, β is the shape parameter, characterizing the dispersion degree of the test data.

$$F(x)=1-\exp\{-(x/\alpha)^{\beta}\} \quad (7)$$

IV. Test Results and Discussion

A. Volume Resistivity Results

Fig. 7 shows the volume resistivities of epoxy samples with each hydrolyzable chlorine content at different hygrothermal aging times (the inset shows the parameters of test electrodes). In the absence of hygrothermal aging treatment, there is a slight increase in the volume resistivity of the epoxy samples with the increasing hydrolyzable chlorine content. This may be caused by the carrier trapping effect of shallow electron traps and deep hole traps in AH-Cl molecules.

Within the hygrothermal aging time of 0 to 48 hours, the volume resistivities of various epoxy samples gradually rise, and the rising extents increase with the increase of the hydrolyzable chlorine content. As mentioned above, the change in molecular structure caused by the hydrolysis of AH-Cl molecules will lead to an increase in the volume resistivity of the material, which is consistent with the test results. As the hydrolyzable chlorine content increases, the contribution of AH-Cl hydrolysis to the elevated volume resistivity increases, and therefore the elevated magnitude of the volume resistivity increases. However, the HCl produced by hydrolysis will cause corrosion to the epoxy sample. The corrosion causes many micro-cavities inside the sample. Compared with that in the resin matrix, the carriers have a greater mobility in the cavities. Therefore, the corrosion of HCl becomes a factor in reducing the volume resistivity of the sample. However, the volume resistivity maintains an increasing tend during the hygrothermal aging time of 0 to 48 hours. Therefore, the corrosion of HCl may not be the main factor affecting the volume resistivity during that aging time.

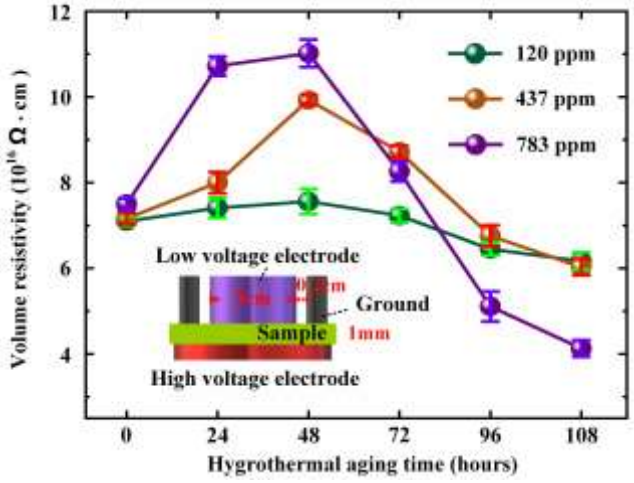

Fig. 7. The variation curves of volume resistivities.

During the hygrothermal aging time of 48 to 108 hours, the volume resistivity of the samples with different hydrolyzable chlorine content are significantly reduced. As the hydrolyzable chlorine content increases, the average decrease rate of volume resistivity increases. These may be due to the intense hydrolysis of AH-Cl molecules during that time period: the corrosion caused by the large amount of HCl turns out to be the main factor weakening the volume resistivity of the material. In addition, the corrosion can cause chain breakage in the resin matrix. The ions and free electrons generated by the breakage also cause a decrease in the volume resistivity. As can be seen, the volume resistivity maintains a decreasing trend during the 48 to 108 hours of hygrothermal aging time.

B. Space Charge Accumulation Characteristics

Fig. 8a and Fig. 8b show the space charge results under the positive polarity voltage. The epoxy samples tested are of a hydrolyzable chlorine content of 783 ppm without aging and after hygrothermal aging for 48 hours. It can be observed that a small amount of positive homo-charge is injected from the anode into both samples, which may be related to the low hole injection barrier of AH-Cl and AH-OH molecules. However, these injected positive charges (holes) seem to migrate more readily in the hygrothermal aged epoxy samples than in the unaged samples. As mentioned above, the overall hole trap depth φ_{th} has a small decrease for AH-OH molecule compared with AH-Cl molecule, which leads to easier migration of holes in the material. This is consistent with the experimental results.

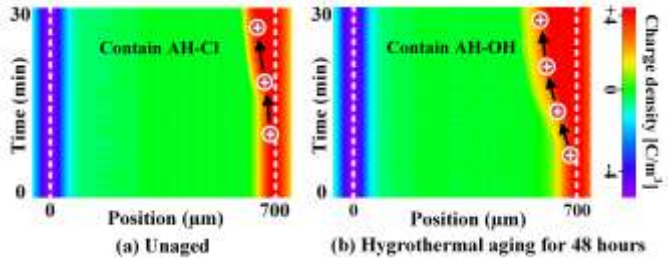

Fig. 8. Space charge results of the samples; (a) unaged; (b) hygrothermal aging for 48 hours.

C. AC Breakdown Strength Results

Fig. 9 shows the AC breakdown strengths of epoxy samples at different hydrolyzable chlorine contents and hygrothermal aging times (the inset shows test schematic), and Fig. 10 shows the Weibull distribution curves of these breakdown strengths. When the epoxy samples are not subjected to hygrothermal aging, the breakdown strength of the samples gradually rises with the increasing hydrolyzable chlorine content, but the rising extent gradually decreases. To explain this phenomenon, we simulated the cross-linking by-product molecule formed in the resin matrix that is similar to the molecular structure of AH-Cl. Compared with the structure of AH-Cl molecule in Fig. 1b-1, the segment A and segment B of the by-product molecule do not change, while the segment C of the molecule becomes the same structure as segment A. Using the same calculation method as above, we obtained the band gap width of the by-product molecule, which is 4.868 eV. While the band gap width of the AH-Cl molecule is 5.065 eV, which can be seen in Fig. 2b. The breakdown is not solely based on electronic behavior, but to some extent, the variation in band gap width can account

for the breakdown behavior. The increase in band gap elevates the energy required for electrons to escape from valence bonds and raises the barrier of electron migration between different lattices [20]. Therefore, the electrons in the AH-Cl molecule are more difficult to escape the bondage of valence bonds and move freely in the material than in the cross-linking by-product molecule. This may explain the higher breakdown strength of the epoxy sample with a higher hydrolyzable chlorine content. However, the presence of hydrolyzable chlorine hinders the curing of the DGEBA/Me-THPA system, which will have a diminishing effect on the intrinsic dielectric strength of the cured resin matrix. Therefore, when the epoxy samples are not subjected to the hygrothermal aging, the rising extent in breakdown strength of the samples reduces as the hydrolyzable chlorine content increases.

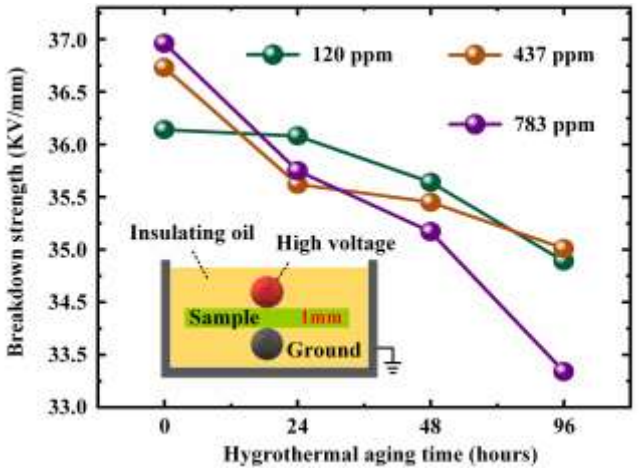

Fig. 9. The variation curves of AC breakdown strengths.

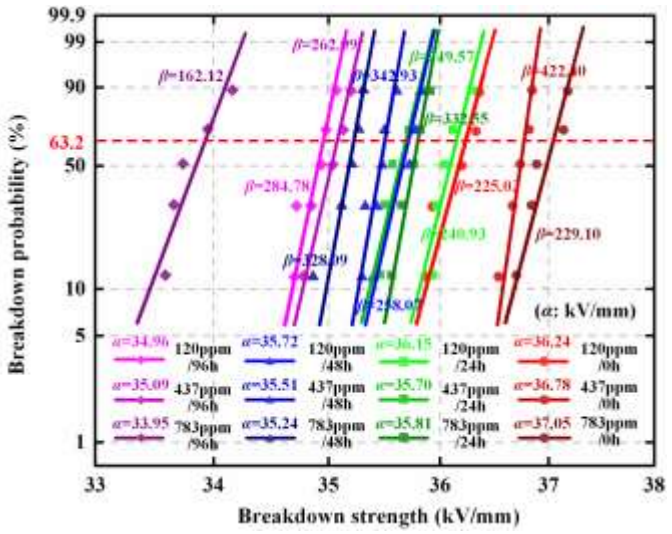

Fig. 10. Weibull fitting curves of AC breakdown strengths.

It can be seen from Fig. 9 that the breakdown strength of epoxy samples with different hydrolyzable chlorine content decreases with the increasing hygrothermal aging times. This may be related to the HCl produced by hydrolysis. Pores are generated inside the sample by the corrosion of the HCl. The electrons in the pores are prone to gain large kinetic energy under the electric field. These electrons with large kinetic energy collide with the resin matrix, making the resin molecular chains susceptible to breakage. As a result, the breakdown strength of the epoxy samples is reduced.

V. Conclusion

We discovered and explained the modulation laws on the molecular orbital energy levels and charge trap depths due to the molecular structural change caused by the hydrolysis of the acid anhydride/chlorohydrin ether molecule, and verified the modulation results using experiments. The overall electron trap depth shows a large increase and the overall hole trap depth shows a small decrease in the hydrolyzed molecule, which resulted in a rising trend of volume resistivity of the epoxy samples after hygrothermal aging. The defects produced by the residual HCl after hydrolysis contributed to the reduction of the breakdown strength of epoxy samples.

In the above work, we have only considered the influence of intra-chain charge trapping sites on the charge transport in the material. However, the inter-chain charge trapping sites are also a factor worth considering, and their formation may be related to the interactions of the inter-chain atoms, which will be given more consideration in our future work.

References

[1] H. Ruan, Q. Xie, J. Yan, J. Song, Z. Zhan, and F. Lü, "Enhanced DC surface insulation of Al_2O_3/ER brought by the permeability of fluorine-containing release agent," *IEEE Trans. Dielectr. Electr. Insul.*, vol. 28, no. 3, pp. 762-770, Jun. 2021.

[2] J. Chen, N. Chu, M. Zhao, F. Jin, and S. Park, "Synthesis and application of thermal latent initiators of epoxy resins: a review," *J. Appl. Polym. Sci.*, vol. 137, no. 48, Dec. 2020, Art. no. e49592.

[3] Y. Zhao, Y. He, K. Yang, X. Wang, J. Bai, and B. Du, "Improving the surface insulating performance of epoxy resin/Al_2O_3 composite materials by extending chain of liquid epoxy resin with Me-THPA," *High Vol.*, vol. 5, no. 4, pp. 472-481, Aug. 2020.

[4] K. Yang *et al.*, "Enhancing dielectric strength of epoxy polymers by constructing interface charge traps," *ACS Appl. Mater. Interfaces.*, vol. 13, no. 22, pp. 25850-25857, Jun. 2021.

[5] J. J. Park, "AC electrical treeing phenomena in an epoxy system with low-chlorine BDGE at various electric field frequencies," *Trans. Electr. Electron. Mater.*, vol. 14, pp. 324-328, Dec. 2013.

[6] L. Chen, H. D. Tran, C. Wang, and R. Ramprasad, "Unraveling the luminescence signatures of chemical defects in polyethylene," *J. Chem. Phys.*, vol. 143, no. 12, Sep. 2015, Art. no. 124907.

[7] A. Huzayyin, S. Boggs, and R. Ramprasad, "Quantum mechanical studies of carbonyl impurities in dielectric polyethylene," *IEEE Trans. Dielectr. Electr. Insul.*, vol. 17, no. 3, pp. 920-925, Jun. 2010.

[8] A. Huzayyin, S. Boggs, and R. Ramprasad, "Density functional analysis of chemical impurities in dielectric polyethylene," *IEEE Trans. Dielectr. Electr. Insul.*, vol. 17, no. 3, pp. 926-930, Jun. 2010.

[9] T. Takada, H. Kikuchi, H. Miyake, Y. Tanaka, M. Yoshida, and Y. Hayase, "Determination of charge-trapping sites in saturated and aromatic polymers by quantum chemical calculation," *IEEE Trans. Dielectr. Electr. Insul.*, vol. 22, no. 2, pp. 1240-1249, Apr. 2015.

[10] M. El-Shahat, A. Huzayyin, and H. Anis, "Effect of chemical impurities on charge injection barriers at the interface of copper and polyethylene," *IEEE Trans. Dielectr. Electr. Insul.*, vol. 26, no. 2, pp. 642-647, Apr. 2019.

[11] J. Li *et al.*, "Effects of high temperature and high electric field on the space charge behavior in epoxy resin for power modules," *IEEE Trans. Dielectr. Electr. Insul.*, vol. 27, no. 3, pp. 882-890, Jun. 2020.

[12] N. Tian *et al.*, "Chloromethyl-modified Ru(ii) complexes enabling large pH jumps at low concentrations through photoinduced hydrolysis," *Chem. Sci.*, vol. 10, no. 43, pp. 9949-9953, Nov. 2019.

[13] M. Meunier and N. Quirke, “Molecular modeling of electron trapping in polymer insulators,” *J. Chem. Phys.*, vol. 113, no. 1, pp. 369-376, Jul. 2000.
[14] L. Chen, T. D. Huan, Y. C. Quintero, and R. Ramprasad, “Charge injection barriers at metal/polyethylene interfaces,” *J. Mater. Sci.*, vol. 51, no. 1, pp. 506-512, Jan. 2016.
[15] K. Yang *et al.*, “Enhancing dielectric strength of thermally conductive epoxy composites by preventing interfacial charge accumulation using micron-sized diamond,” *Compos. Sci. Technol.*, vol. 221, Apr. 2022, Art. no. 109178.
[16] W. Wang, T. Takada, Y. Tanaka, and S. Li, “Space charge mechanism of polyethylene and polytetrafluoroethylene by electrode/dielectrics interface study using quantum chemical method,” *IEEE Trans. Dielectr. Electr. Insul.*, vol. 24, no. 4, pp. 2599-2606, Aug. 2017.
[17] K. Toyoda, Y. Nakano, I. Hamada, K. Lee, S. Yanagisawa, and Y. Morikawa, “First-principles study of the pentacene/Cu (111) interface: adsorption states and vacuum level shifts,” *J. Electron Spectrosc. Relat. Phenom.*, vol. 174, pp. 78-84, Aug. 2009.
[18] C. Han, B. Du, J. Li, Z. Li, and T. Tanaka, “Investigation of charge transport and breakdown properties in XLPE/GO nanocomposites part 1: The role of functionalized GO quantum wells,” *IEEE Trans. Dielectr. Electr. Insul.*, vol. 27, no. 4, pp. 1204-1212, Aug. 2020.
[19] C. Han, B. Du, J. Li, Z. Li, and T. Tanaka, “Investigation of charge transport and breakdown properties in XLPE/GO nanocomposites part 2: Effect of polarity reversal,” *IEEE Trans. Dielectr. Electr. Insul.*, vol. 27, no. 4, pp. 1213-1221, Aug. 2020.
[20] J. Li, Y. Wang, Z. Ran, H. Yao, B. Du, and T. Takada, “Molecular structure modulated trap distribution and carrier migration in fluorinated epoxy resin,” *Mol.*, vol. 25, no. 13, Jul. 2020, Art. no. 3071.

Yushun Zhao was born in Shandong Province, China. He received the M.S. and Ph.D. degrees in material physics and chemistry and electrical engineering from Chongqing University, Chongqing, China, in 2007 and 2010, respectively.

He is currently an associate professor of high voltage and insulation technology department at Hefei University of Technology. His major research interests include new electrical materials, electrical insulation design, power equipment online monitoring and fault diagnosis, power system lightning and overvoltage protection.

Mr. Zhao is a member of the equipment insulation group of the High Voltage Professional Committee of the Chinese Society of Electrical Engineering and an academic committee member of a Key Laboratory of Aviation Science and Technology.

Gilbert Teyssèdre was born in May 1966 in Rodez, France. He received his engineer degree in materials physics and graduated in solid state physics in 1989 at the National Institute for Applied Science (INSA), Toulouse, France. Then he obtained the Ph.D. degree from Paul Sabatier University, Toulouse, France in 1993 for a work on ferroelectric polymers at the Solid State Physics Lab.

He entered the CNRS in 1995 and has been working since then at the Electrical Engineering Lab (now LAPLACE) in Toulouse. He is currently Research Director at CNRS and is leading a team working on the reliability of dielectrics in electrical equipment. His research activities concern the development of luminescence techniques in insulating polymers with focus on chemical and physical structure, degradation phenomena, space charge and transport properties.

Mr. Teyssèdre is member of the scientific committee of several conference series as CEIDP since 2016, ICD, ICEMPE, and JiCable. He is Associate Editor of IEEE Trans. Dielectr. Electr. Insul (2021-).

Bin Du was born in Shandong Province, China. He received the Ph.D. degree in electrical engineering from Chongqing University, Chongqing, China, in 2016.

He is currently working at Hefei University of Technology. His major research interests include new electrical materials, electrical insulation design, power equipment online monitoring and fault diagnosis.